

Journal of Materials Chemistry A

Accepted Manuscript



This is an *Accepted Manuscript*, which has been through the Royal Society of Chemistry peer review process and has been accepted for publication.

Accepted Manuscripts are published online shortly after acceptance, before technical editing, formatting and proof reading. Using this free service, authors can make their results available to the community, in citable form, before we publish the edited article. We will replace this *Accepted Manuscript* with the edited and formatted *Advance Article* as soon as it is available.

You can find more information about *Accepted Manuscripts* in the [Information for Authors](#).

Please note that technical editing may introduce minor changes to the text and/or graphics, which may alter content. The journal's standard [Terms & Conditions](#) and the [Ethical guidelines](#) still apply. In no event shall the Royal Society of Chemistry be held responsible for any errors or omissions in this *Accepted Manuscript* or any consequences arising from the use of any information it contains.

Cite this: DOI: 10.1039/c0xx00000x

ARTICLE TYPE

www.rsc.org/xxxxxx

Bicontinuous Hierarchical Na₇V₄(P₂O₇)₄(PO₄)/C Nanorod-Graphene Composite with Enhanced Fast Sodium and Lithium Ions Intercalation Chemistry

Sen Zhang^{*a}, Chao Deng^{*b} and Yu Meng^a

Received (in XXX, XXX) Xth XXXXXXXXXX 20XX, Accepted Xth XXXXXXXXXX 20XX

DOI: 10.1039/b000000x

Mixed polyanion materials with 3D framework as battery electrodes are drawing enormous attention recently in view of the requirement on further improving energy storage and power densities. Here we present a design of hierarchical Na₇V₄(P₂O₇)₄(PO₄)/C nanorod-graphene composite as sodium- and lithium-storage cathode material. The hierarchical structure is composed of 1D rectangle Na₇V₄(P₂O₇)₄(PO₄)/C nanorod which is coated by *in-situ* residual carbon and wrapped by reduced graphene-oxide sheet. The open network of graphene and surface carbon coating of Na₇V₄(P₂O₇)₄(PO₄)/C nanorod provide bicontinuous electron and ion pathways, which constructs a three-dimensional conductive network for efficient electron and ion transfer. The flexible electrode built from the hierarchical composite free of binder or conductive additive exhibits improved electron conductivity and higher sodium/lithium ion migration coefficients than the pristine Na₇V₄(P₂O₇)₄(PO₄)/C nanorod. It approaches the initial reversible electrochemical capacities of 91.4 and 91.8 mAh·g⁻¹ with high discharge potentials over 3.8 V (vs. Na/Na⁺ or Li/Li⁺) and good cycling property with capacity retentions of 95% and 83% after 200 cycles at 1C rate in sodium and lithium intercalation systems, respectively. Even at 10 C, it still delivers 87.4% (for sodium) and 78.2% (for lithium) of the capacity and high cycling stability. Given the compatibilities of both sodium/lithium ions and superior electrochemical characteristics, the bicontinuous hierarchical composite is considered to be a promising high-property electrode material for advanced energy storage applications.

Keyword: Na₇V₄(P₂O₇)₄(PO₄)/C nanorod; bicontinuous pathways; hierarchical nanoarchitecture; sodium/lithium ion migration; superior electrochemical property

1 Introduction

The tremendous battery requirements for electric vehicles (EV) and large scale grid-based electric energy storage (EES) demand intensive exploration of electrode materials, in terms of high energy density, high power density, long cycle life, safety and low cost¹. Based on these issues, electroactive materials with three-dimensional framework and flexible ion channels have attracted intensive interests. In the past decades, various 3D framework materials including metal oxides^{2,3}, polyanion materials⁴⁻⁷, fluoride-based materials^{8,9} and metal-organic materials¹⁰⁻¹² have been synthesized. The exploration of these materials impels the fast development of the batteries based on ion intercalation chemistry.

Among the present 3D-framework materials, polyanion materials are considered to be one of the most promising candidates. Since the introduction of LiFePO₄ in 1980s, various polyanion-based materials such as silicates (A₂MSiO₄)^{7,13},

borates (AMBO₃)¹⁴, phosphates (AMPO₄)⁴⁻⁶, pryphosphates (AMP₂O₇)^{15,16}, fluorophosphates (AMPO₄F)¹⁷, and so on, have been extensively studied. However, within the limited kinds of polyanion groups, the development of “single” polyanion materials is greatly restricted. Recently, mixed-polyanion materials with 3D framework have come into sight as a new member of the polyanion family¹⁸⁻²⁸. Compared with single-polyanion materials, the flexible design of mixed-polyanion materials dramatically expand the research scope and provides new opportunities for polyanion materials. A series of mixed-polyanion materials such as Na₄Fe₃(PO₄)₂(P₂O₇)^{18,19}, Na₄Co₃(PO₄)₂(P₂O₇)²⁰, Li₉V₃(P₂O₇)₃(PO₄)₂^{21,22}, Li_{1-x}Fe_{1+x}P_xSi_{1-x}O₄^{23,24}, Li_{2+x}Mn_{1-x}P_xSi_{1-x}O₄²⁵ et al have been investigated. Especially, introduced by lim et al^{26,27}, a very recently reported vanadium-based mixed-polyanion compound Na₇V₄(P₂O₇)₄(PO₄)²⁸ has attracted great interest. As illustrated in Figure 1, the 3D framework of [V₄(P₂O₇)₄(PO₄)]_∞ is constructed through each [PO₄] tetrahedron sharing corners with four adjacent [VO₆] octahedrons and each [P₂O₇] group sharing corners with two

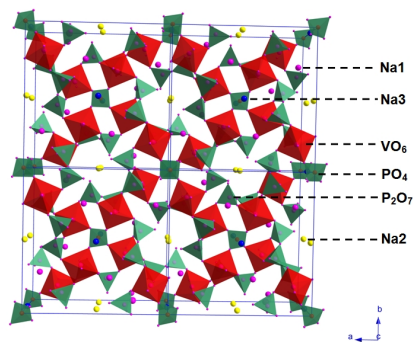


Figure 1 Crystal structure of $\text{Na}_7\text{V}_4(\text{P}_2\text{O}_7)_4(\text{PO}_4)$

adjacent $[\text{VO}_6]$ octahedrons^{26,27}. Three different interstitial sites (i.e., Na1, Na2, and Na3) are occupied by sodium ions. Therefore, sodium/lithium ions can diffuse along the well-defined channels in the 3D framework, which enables the fast de/intercalation of sodium/lithium ions. Therefore, the well defined 3D framework structure as well as open ion diffusion channels and high operating potential makes it a promising electrode material candidate. However, facing the same problem as other polyanion materials, the inferior conductivity restricts its fast electrochemical kinetic and rate capability. Thus further improvement on its high rate performance is still a big challenge.

For a “rocking chair” battery, ion and electron transport capabilities are the determining factors to its electrochemical properties especially at high rates. Tailoring materials into nanosize is one of the most effective strategies to improve ion diffusion kinetic and then enhance its rate performance. Among the wide range of nanostructures, 1D nanostructure with short ion diffusion distance as well as continuous electron transport pathway has demonstrated superiority in energy storage applications²⁹⁻³¹. Based on this viewpoint, we have successfully designed and synthesized 1D nanostructured $\text{Na}_7\text{V}_4(\text{P}_2\text{O}_7)_4(\text{PO}_4)/\text{C}$ nanorod with stable cycling stability in recent report³². However, the poor connectivity between random distributed nanorods provides inconsecutive pathways for electron transport, which restricts its high rate property. Therefore, in order to meet ever increasing demand for high power applications, it is highly desirable to design 3D hierarchical architecture combining both active materials and conductive scaffolds to construct continuous electron/ion pathways for further improvements. Carbon matrix can effectively provide a conductive network for electrode materials. Mai's group have used several kind of carbon matrix to improve the conductivity of electrode materials^{33,34}. These carbon matrices can significantly improve the electronic/ionic conductivity. Therefore, it is desirable for us to employ a 3D carbon matrix to improve the conductivity of the $\text{Na}_7\text{V}_4(\text{P}_2\text{O}_7)_4(\text{PO}_4)/\text{C}$ nanorod.

Following this viewpoint, as illustrated in Figure 2, herein we present the construction of bicontinuous hierarchical $\text{Na}_7\text{V}_4(\text{P}_2\text{O}_7)_4(\text{PO}_4)/\text{C}$ nanorod-graphene composite. The hierarchical structure is composed of 1D rectangle

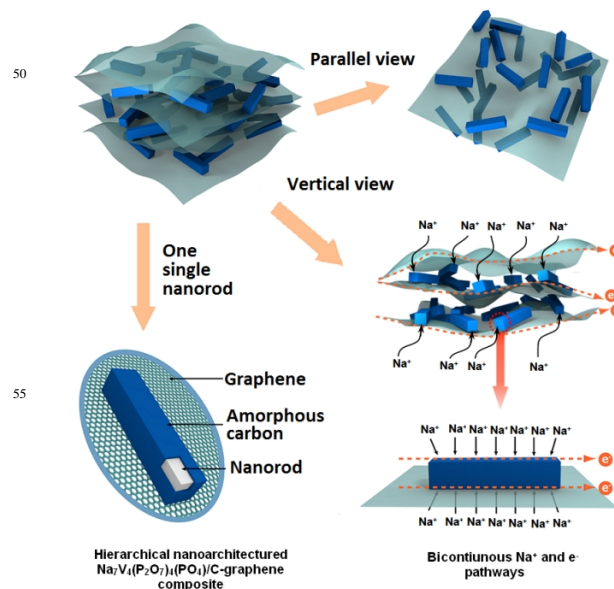


Figure 2 Schematic illustration of the hierarchical $\text{Na}_7\text{V}_4(\text{P}_2\text{O}_7)_4(\text{PO}_4)/\text{C}$ nanorod-graphene composite with bicontinuous electron/ion transport pathways. The parallel and vertical view of one layer and the image of one single nanorod are enlarged.

$\text{Na}_7\text{V}_4(\text{P}_2\text{O}_7)_4(\text{PO}_4)/\text{C}$ nanorod which is coated by *in-situ* residual carbon and enclosed by 2D graphene nanosheet scaffolds. The open network of conductive graphene and surface coating of *in-situ* carbon construct bicontinuous electron and ion pathways for the $\text{Na}_7\text{V}_4(\text{P}_2\text{O}_7)_4(\text{PO}_4)/\text{C}$ nanorod. Thus such advantages as large surface area, improved conductivity and rapid electron and ion transfer have been expected for the hierarchical architecture. Inspired by these advantages, the compatibilities of sodium and lithium intercalation chemistry on hierarchical $\text{Na}_7\text{V}_4(\text{P}_2\text{O}_7)_4(\text{PO}_4)/\text{C}$ electrode were investigated for the first time. The flexible binder-free electrode based on hierarchical $\text{Na}_7\text{V}_4(\text{P}_2\text{O}_7)_4(\text{PO}_4)/\text{C}$ composite demonstrates impressive high rate property, superior cyclability and high operating potential in both sodium/lithium intercalation systems. The superior electrochemical characteristics and good compatibilities of sodium/lithium ions demonstrate the significant potential of it as a high-energy storage electrode for “rocking chair” batteries.

2 Experimental

2.1 Synthesis.

The 1D nanostructured $\text{Na}_7\text{V}_4(\text{P}_2\text{O}_7)_4(\text{PO}_4)/\text{C}$ nanorod is prepared by a molten-salt synthetic strategy as details in previous reports³². Briefly, Stoichiometric amount of NH_4VO_3 , NaHCO_3 , $\text{NH}_4\text{H}_2\text{PO}_4$ and desired amount of citric acid were mixed to form a homogenous solution. The molar ratio of citric acid to NaHCO_3 is 1:3. The resulting solution was kept at 80 °C under magnetic stirring to evaporate water until it turned into a wet gel. The wet

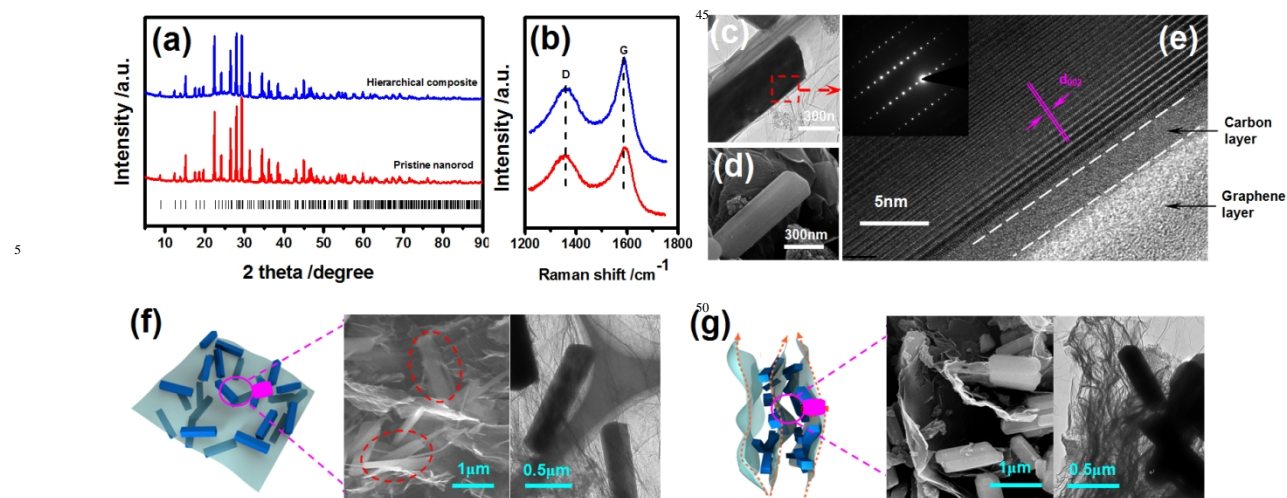


Figure 3 Comparison of (a) XRD and (b) Raman between the pristine nanorod and the hierarchical composite. (c) TEM and (d) SEM images of a single $\text{Na}_7\text{V}_4(\text{P}_2\text{O}_7)_4(\text{PO}_4)$ nanorod. (e) HRTEM image of the single nanorod enlarged in red square of (c), and the corresponding SEAD pattern is shown as an inset. SEM and TEM images of hierarchical $\text{Na}_7\text{V}_4(\text{P}_2\text{O}_7)_4(\text{PO}_4)$ nanorod-graphene composite with parallel (f) and vertical (g) view of schematic diagrams.

gel was dried over night to obtain the dry gel which was grounded and subjected to programmed heat treatment at 850 °C for 12 h, cooled to 500 °C at the rate of 1 °C min^{-1} and quenched to room temperature in an argon atmosphere. The quenching process is employed to avoid the decomposition of the target compound and the precipitation of more crystalline phases. No chemical reaction is involved in the quenching process. The resulting intermediate product was soaked in hot water with argon bubbling. The soaking process can eliminate the Na-P-O salts which coexist with the target compound, and bubbling Ar can get rid of the oxygen dissolved in water to prevent the oxidation of the target compound. The chemical reactions involved in the soaking process are the hydrolysis of the Na-P-O salts. The Na-P-O salts are a mixture of crystalline and amorphous compounds, for example NaPO_3 and $\text{Na}_4\text{P}_2\text{O}_7$, which composition is unclear. After filtering, washing and drying, the $\text{Na}_7\text{V}_4(\text{P}_2\text{O}_7)_4(\text{PO}_4)/\text{C}$ nanorod was obtained.

Graphene was produced by the reduction of graphene oxide prepared by a modified Hummer's method and the binder-free thin film was prepared by ultrafiltration as details in literatures^{35,36}. The hierarchical $\text{Na}_7\text{V}_4(\text{P}_2\text{O}_7)_4(\text{PO}_4)/\text{C}$ nanorod-graphene composite was prepared via two simple steps. Firstly, stock solution of dispersed graphene (20 wt.%) was mixed with the $\text{Na}_7\text{V}_4(\text{P}_2\text{O}_7)_4(\text{PO}_4)/\text{C}$ nanorod (80 wt.%), and the mixture was dispersed under ultrasonic wave for one hour. Then the dispersion was vacuum ultrafiltered and washed with excess of DI water. The thin film electrode was obtained after dried, and then it was treated at 120 °C for 24 hours in vacuum before work in the sodium ion battery. The thickness of the binder free film is 24 μm. The loading of the active mass in the graphene-containing electrode is about 3.15 $\text{mg}\cdot\text{cm}^{-2}$. The pristine nanorod electrode

was made from a mixture of the pristine nanorod, acetylene black and polyvinylidene fluoride (PVDF) in a weight ratio of 80:10:10. The loading of the active mass in the PVDF-bound electrode is about 3.42 $\text{mg}\cdot\text{cm}^{-2}$. The weight of graphite or carbon is deducted to obtain the loading of the active mass.

2.2 Materials characterization

Powder X-ray diffraction (XRD, Bruker D8/Germany) using Cu K α radiation was employed to identify the crystalline phase of the material. The experiment was performed by using step mode with a fixed time of 3 s and a step size of 0.02°. The morphology was observed with a scanning electron microscope (SEM, HITACHI S-4700) and a transmission electron microscope (TEM, JEOS-2010 PHILIPS). Raman spectra of the composites were collected on a Jobin-Yvon Labor Raman system by exciting a 514.5 nm Ar ion laser (Raman, HR-800 HORIBA). The carbon content was determined by an elemental analyzer (EA, Elementar Vario EL). The electronic conductivity was measured on the disk of nanorod and the thin film of hierarchical composite by four probe technique. The nanorod powder was pressed into a disk with a diameter of 20 mm and a thickness of about 0.5 mm at a pressure of 10 MPa, then gold was painted on both sides of the disk and the thin film electrode to ensure electrical contact. The carbon content in the $\text{Na}_7\text{V}_4(\text{P}_2\text{O}_7)_4(\text{PO}_4)/\text{C}$ nanorod is about 1.48 wt%, which is determined by an element analyzer (EA, Elementar Vario EL).

2.3 Electrochemical measurements

The electrochemical performance was carried out using coin type cells. For the sodium intercalation system, the Na foil was employed as counter and reference electrode and 1 $\text{mol}\cdot\text{L}^{-1}$

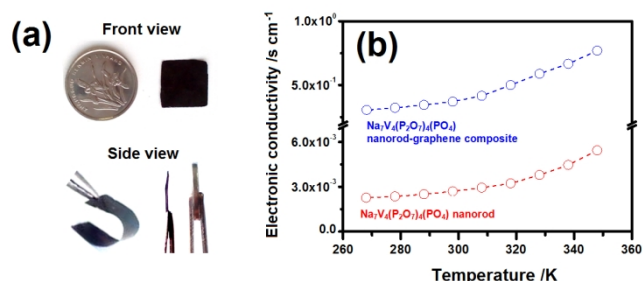


Figure 4 (a) Front view and side view of the flexible and binder free $\text{Na}_7\text{V}_4(\text{P}_2\text{O}_7)_4(\text{PO}_4)/\text{C}$ nanorod-graphene thin film. (b) The temperature dependence of electronic conductivity of the $\text{Na}_7\text{V}_4(\text{P}_2\text{O}_7)_4(\text{PO}_4)/\text{C}$ nanorod-graphene film and the $\text{Na}_7\text{V}_4(\text{P}_2\text{O}_7)_4(\text{PO}_4)/\text{C}$ nanorod pellet.

NaClO_4 dissolved in propylene carbonate (PC) was used as electrolyte. For the lithium intercalation system, the Li foil was employed as counter and reference electrode and 1 mol L^{-1} LiPF_6 dissolved in the mixture of ethylene carbonate (EC) and dimethyl carbonate (DMC) was used as electrolyte. Galvanostatic charge-discharge tests were performed in the potential range of 2.5~4.1 V vs. Na/Na^+ and 2.5~4.3 V vs. Li/Li^+ at ambient temperature on a Land battery testing system (Wuhan, China). EIS measurements were conducted at a fully discharged state using a Zivelab electrochemical workstation, and the applied frequency range is 100k~0.05 Hz.

3 Results and Discussion

Figure 3(a) shows the XRD pattern of the hierarchical $\text{Na}_7\text{V}_4(\text{P}_2\text{O}_7)_4(\text{PO}_4)/\text{C}$ -graphene composite and the pristine $\text{Na}_7\text{V}_4(\text{P}_2\text{O}_7)_4(\text{PO}_4)/\text{C}$ nanorod. All the diffraction peaks can be readily indexed to the tetragonal phase (space group: $P-42_1c$) without impurity phases, indicating the high purity of both materials. The uneven background of XRD pattern for the hierarchical composite displays a broad diffraction peaks at $\sim 24^\circ$, corresponding to the average d -spacing of graphene layers³⁷. The Raman spectra (Figure 2b) identify two characteristic signatures located at 1357 and 1589 cm^{-1} for both materials, corresponding to the D (disordered carbon) and G (graphene carbon) bands^{38,39}. The higher intensity of G band and lower value of the D/G intensity ratio were observed for the hierarchical composite in comparison with those of the pristine nanorod, demonstrating its higher sp^2 domain size.

The morphology and microstructure of the hierarchical composite were investigated by SEM and TEM. As shown in Figure 3(c)~(g), rectangle shaped nanorod with diameter of 200~300 nm and the length of 1~2 μm are encompassed by the graphene sheets, which results in the hierarchical architecture of the composite. The enlarged parallel view of the composite (Figure 3f) demonstrates that the $\text{Na}_7\text{V}_4(\text{P}_2\text{O}_7)_4(\text{PO}_4)/\text{C}$ nanorods are well wrapped up by graphene sheet layer by layer. And the enlarged vertical view (in Figure 3g) suggests the nanorods tend to lie with length parallel to the graphene surface. The large

graphene sheets build 3D conductive framework for the stacking nanorods, which provides intimate contact between each other and construct continuous electron transport pathways. The architecture of one single nanorod is further identified by high resolution TEM (HRTEM). As shown in insert of Figure 3(e), the corresponding selected area electron diffraction (SEAD) patterns reveals that the $\text{Na}_7\text{V}_4(\text{P}_2\text{O}_7)_4(\text{PO}_4)/\text{C}$ nanorod are single crystalline. The well-resolved lattice fringe with the interplanar distance of 0.3198 nm corresponding to the (002) lattice planes of the $\text{Na}_7\text{V}_4(\text{P}_2\text{O}_7)_4(\text{PO}_4)$. Additionally, a nanolayer of 3 nm on the surface of the nanorod is clearly observed, which comes from the residual amorphous carbon and constructs a continuously electron transport pathways along the nanorod surface. Therefore, both the surface conductive layer and the 3D conductive framework construct bicontinuous electron pathways and facilitates fast electrochemical kinetic.

Moreover, the hierarchical architecture also enhances the mechanical strength of the composite, which enable the formation of flexible electrodes, free of both binder and conducting additives (Figure 4a). The electronic conductivity of both the binder-free hierarchical composite film and the pristine $\text{Na}_7\text{V}_4(\text{P}_2\text{O}_7)_4(\text{PO}_4)/\text{C}$ nanorod pellets were investigated. The electron conductivities of both films are compared in Figure 4(b). The hierarchical composite possessed good conductivity in the temperature change from -5°C to 65°C with slight change from 0.30 s cm^{-1} to 0.76 s cm^{-1} , which is about two orders higher than that of the pristine nanorod pellets (from $2.27 \times 10^{-3} \text{ s cm}^{-1}$ to $5.41 \times 10^{-3} \text{ s cm}^{-1}$). By virtue of the 3D conductive framework, the improved electron conductivity of hierarchical composite makes possible embodiment of outstanding electrochemical performance.

Inspired by the advantages of hierarchical architecture, the sodium and lithium ion intercalation chemistry of the $\text{Na}_7\text{V}_4(\text{P}_2\text{O}_7)_4(\text{PO}_4)/\text{C}$ -graphene composite was investigated. The application of the $\text{Na}_7\text{V}_4(\text{P}_2\text{O}_7)_4(\text{PO}_4)$ in lithium ion battery with hybrid-ion migration has two potential advantage. Firstly, the natural abundance of sodium can make the Na-containing compounds cheaper than the lithium-containing compounds. Secondly, the standard electrode potential of lithium metal is lower than that of sodium metal, thus the use of $\text{Na}_7\text{V}_4(\text{P}_2\text{O}_7)_4(\text{PO}_4)$ in lithium ion battery can result in a higher voltage. First of all, the galvanostatic charge-discharge characteristics of the hierarchical composite in the sodium and lithium batteries were investigated. As displayed in Figure 5(a), the hierarchical composite exhibits initial capacity of 91.4 mAh g^{-1} at the rate of C/20 in the sodium ion battery. Two charge plateaus and one discharge plateau are observed in the charge/discharge curves, corresponding well to two oxidation (3.883 V and 3.933 V vs. Na^+/Na) and one reduction (3.861 V vs. Na^+/Na) peaks in the differential capacity curves (Figure 5b). The splitting of charge plateaus indicates the existence of intermediate phase, which agrees well with those reported by Lim et al^{26,27}. The shape of galvanostatic curves changes slightly during cycles and as high as 98.2% of capacity retention was obtained after one

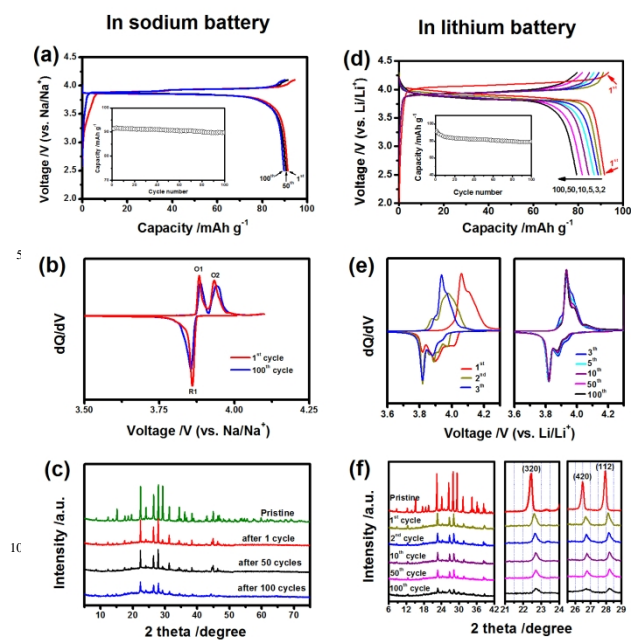


Figure 5 Galvanostatic charge/discharge curves (a, d) and the corresponding differential capacity curves (b, e) of the hierarchical $\text{Na}_7\text{V}_4(\text{P}_2\text{O}_7)_4(\text{PO}_4)/\text{C}$ nanorod-graphene electrode in sodium (a, b) and lithium (d, e) intercalation systems. The cycling properties are shown as insets of (a) and (d). *Ex-situ* XRD patterns of the electrode after 1, 2, 10, 50 and 100 cycles in (c) sodium and (f) lithium batteries. The (320), (420) and (112) peaks in (f) are enlarged.

hundred cycles (inset of Figure 5a). Moreover, *Ex-situ* XRD patterns also identify the similar structure between the pristine and cycled materials, which demonstrates the good structure reversibility of $\text{Na}_7\text{V}_4(\text{P}_2\text{O}_7)_4(\text{PO}_4)/\text{C}$ during sodium intercalation (Figure 4c).

As for the lithium intercalation system, the ion transport process becomes more complex. As displayed in Figure 5(d) and (e), the initial cycle is very different from following ones with obvious higher charge/discharge potentials and distinct redox peaks. Two oxidation peaks located at 4.057 and 4.108 V vs Li^+/Li was observed in the initial charge, coincided with the Na extraction process from crystal structure of $\text{Na}_7\text{V}_4(\text{P}_2\text{O}_7)_4(\text{PO}_4)/\text{C}$. In the subsequent discharge process, the appearance of three reduction peaks suggests of hybrid insertion process involving both Na and Li ions. The redox peaks gradually shift with altering the shape of potential plateaus in the following cycles, and become stable after five to ten cycles. Additionally, the capacities also change accompanying with alteration of redox peaks. As displayed in inset of Figure 5(d), the composite approaches the highest capacity of $91.8 \text{ mAh}\cdot\text{g}^{-1}$ in the initial cycle, and then it quickly turns to decrease and becomes stable after five to ten cycles. Similar phenomenon has been observed by Barker, Nazar and Banks et al in previous reports^{20,40-44}, who have operated the sodium intercalated materials such as $\text{Na}_3\text{V}_2(\text{PO}_4)_2\text{F}_3$,

$\text{Na}_3\text{V}_2(\text{PO}_4)_3$ and NaVPO_4F in a lithium based electrolyte and discovered the new hybrid ion batteries (HIB). Based on the rocking chair chemistry of HIB, the initial higher potential with capacity fading in initial a few cycles is associated with the initially temporary disorder induced by hybrid de/insertion process, which has been suppressed and reformed by the predominately Li ion transport in the sequential cycles due to a vast excess of $\text{Li}^{20,38-42}$. Thus gradual capacity alteration process in initial cycles indicates the transformation process from the hybrid ions (sodium and lithium) transport mechanism to the lithium dominate transport mechanism. And the final stabilization suggests the completion of the transformation process. Evidences from the *ex-situ* XRD patterns also support the intercalation process. As displayed in Figure 5(f), obvious right shift was observed in the XRD patterns after initial cycle, which suggests crystal volume decrease in initial cycle. Then the right shift of the XRD patterns become slowly in following cycles and the peak positions stabilized after ten cycles, indicating the structure reconstruction process during hybrid ion intercalation. The similarity between the XRD patterns after ten cycles also demonstrates the good reversibility for lithium intercalation after initial structure adjustment. It also results in the high capacity retention of 94% from ten to one hundred cycles (inset of Figure 5d). Therefore, all of above results demonstrate that the $\text{Na}_7\text{V}_4(\text{P}_2\text{O}_7)_4(\text{PO}_4)/\text{C}$ composite can be employed as the host material for Li as well as Na.

Motivated by the good compatibilities of Na/Li ion, the high rate capability and cycling stability of both pristine $\text{Na}_7\text{V}_4(\text{P}_2\text{O}_7)_4(\text{PO}_4)$ nanorod and the hierarchical $\text{Na}_7\text{V}_4(\text{P}_2\text{O}_7)_4(\text{PO}_4)/\text{C}$ -graphene composite in sodium/lithium ion batteries were investigated. A series of current densities, from 0.05 C to 30 C are employed to evaluate the rate capability. In order to reduce the effect of the capacity fading on the C-rate test, the C-rate test is conducted after three previous charge-discharge cycling. As compared in Figure 6(a) and (d), the pristine nanorod exhibits higher capacities than the hierarchical composite as the current density is lower than 0.5C in both sodium/lithium systems. When the current is higher than 0.5 C, obviously higher capacities were observed for the hierarchical composite than the pristine nanorods in both systems. As the current density increases, the difference between two cathode materials becomes more significant. For example, at the 10 C and 20 C rates in sodium battery, the capacities of 80.2 and $70.3 \text{ mAh}\cdot\text{g}^{-1}$ corresponding to 87.4% and 76.9% of capacity at 0.05C are realized for the hierarchical composite, which is much higher than the pristine nanorods (71.2 and $54.5 \text{ mAh}\cdot\text{g}^{-1}$). Compared with sodium ion battery, both electrode materials exhibit inferior properties in lithium ion battery, especially at high rate (Figure 6b and e). At 20 C rate, the hierarchical composite exhibits the capacity of $70.3 \text{ mAh}\cdot\text{g}^{-1}$ in sodium ion battery, which is higher than the capacity of $54.2 \text{ mAh}\cdot\text{g}^{-1}$ in lithium ion battery. The long-term cycling performance of both materials at the 1 C rate is shown in Figure 6(c) and (f). The capacity retentions of hierarchical composite are 95% and 83% for sodium and lithium

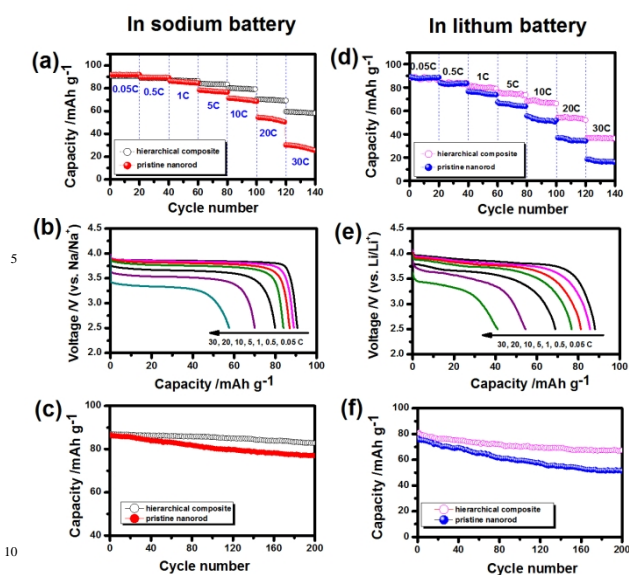


Figure 6 Rate capability of the hierarchical $\text{Na}_7\text{V}_4(\text{P}_2\text{O}_7)_4(\text{PO}_4)/\text{C}$ nanorod-graphene composite and the pristine $\text{Na}_7\text{V}_4(\text{P}_2\text{O}_7)_4(\text{PO}_4)/\text{C}$ nanorod in sodium (a) and lithium (d) intercalation system. The galvanostatic charge/discharge curves of the hierarchical $\text{Na}_7\text{V}_4(\text{P}_2\text{O}_7)_4(\text{PO}_4)/\text{C}$ nanorod-graphene composite at different current densities in sodium (b) and lithium (e) intercalation systems. Long-term cycling properties of the hierarchical $\text{Na}_7\text{V}_4(\text{P}_2\text{O}_7)_4(\text{PO}_4)/\text{C}$ nanorod-graphene composite and the pristine $\text{Na}_7\text{V}_4(\text{P}_2\text{O}_7)_4(\text{PO}_4)/\text{C}$ nanorod at the 1 C rate in (c) sodium and (f) lithium batteries.

systems respectively after cycles, which are higher than those of the pristine one (89% for sodium and 68% for lithium system).

In order to reveal the origin of different behaviors for pristine nanorod and hierarchical composite in both systems, the electrochemical impedance spectra (EIS) of are investigated and the results are summarized in Figure 7 (a) and (b). The measurements were carried out on the materials after all the cycles and the Nyquist plots are displayed in Figure 7 (c). The hierarchical composite exhibits smaller high frequency semicircles than the pristine one in both systems, indicating its improved contact conductivity. For the same material, the sodium system obtains smaller high-frequency semicircle than the lithium system, which suggests its smaller electrochemical resistance. In comparison with the sodium batteries, the higher charge transfer resistance (R_{ct}) of the lithium batteries can be attributed to the structural change induced by Li^+ intercalation. The structural change occurs when Li^+ intercalates instead of Na^+ in the initial few cycles. The Nyquist plots reveal the detrimental effect of the structural change on charge transfer reaction. Based on the low frequency sloping line, the apparent ion diffusion coefficients are calculated (with detailed process in S1)⁴⁵⁻⁴⁷. The linear relationship between Z'' and the reciprocal square root of

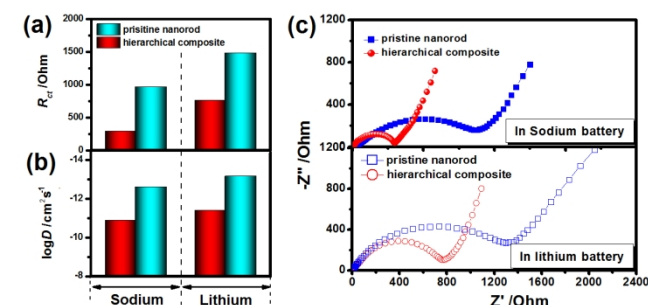


Figure 7 Comparison of the charge transfer resistance (a) and the apparent ion diffusion coefficients (b) between the $\text{Na}_7\text{V}_4(\text{P}_2\text{O}_7)_4(\text{PO}_4)/\text{C}$ nanorod-graphene composite and the pristine $\text{Na}_7\text{V}_4(\text{P}_2\text{O}_7)_4(\text{PO}_4)/\text{C}$ nanorod in sodium and lithium batteries. (c) Nyquist plots of the hierarchical composite and the pristine nanorod in both sodium and lithium batteries.

frequency in low frequency are showed in Figure S2. Both D_{Na} and D_{Li} of the hierarchical composite are higher than those of the pristine one, suggests the improved ion transport capability of the hierarchical architecture. As for the same material, the D_{Li} are lower than D_{Na} , which demonstrates the lower kinetic of lithium insertion and leads to inferior rate capability in lithium intercalation system.

According to the rate capability, the lithium intercalation kinetics of the $\text{Na}_7\text{V}_4(\text{P}_2\text{O}_7)_4(\text{PO}_4)/\text{C}$ nanorod is inferior to its sodium intercalation kinetics. Similar phenomena were already reported for some sodium-containing compounds, for example $\text{Na}_{1.4}\text{Co}_3(\text{PO}_4)_2\text{P}_2\text{O}_7$, $\text{Na}_3\text{V}_2(\text{PO}_4)_3$ and $\text{Na}_3\text{V}_2(\text{PO}_4)_2\text{F}_3$ ^{20,40-44}, when the testing systems enable hybrid ion migration. Although the radius of Li^+ is much smaller than the radius of Na^+ , the charge density of Li^+ is much higher than the charge density of Na^+ because both valence states are +1. When Li^+ intercalates instead of Na^+ , the higher charge density of Li^+ triggers the structural change of the host, which worsens the rate capability.

On the basis of above results, the superb rate capability and better cycling property of hierarchical $\text{Na}_7\text{V}_4(\text{P}_2\text{O}_7)_4(\text{PO}_4)/\text{C}$ composite can be attributed to the advantages of the hierarchical architecture as illustrated in Figure 1. Firstly, both 3D conductive framework and surface carbon coating provide bicontinuous electron/ion pathway as well as large surface area and short ion diffusion channel, which facilitate fast ion diffusion. Additionally, improved connectivity between single $\text{Na}_7\text{V}_4(\text{P}_2\text{O}_7)_4(\text{PO}_4)/\text{C}$ nanorods and the large graphene framework effectively improve the mechanical strength of the composite, which results in formation of flexible binder-free electrode with improved conductivity and superior high rate capability. Furthermore, the hierarchical architecture guarantees the effective electron contact upon prolonged cycling, which facilitates the high-rate cycling stability. Therefore, all these advantages result in the enhanced electrochemical performance of the hierarchical structured composite.

4 Conclusions

In summary, we construct a hierarchical structured Na₇V₄(P₂O₇)₄(PO₄)/C nanorod-graphene composite as electrode materials for sodium and lithium intercalation systems. The large graphene nanosheet constructs 3D framework for the Na₇V₄(P₂O₇)₄(PO₄)/C nanorods, which provides bicontinuous electron/ion transport pathways and large electrolyte-electrode contact area for rapid electron/ion diffusion. Moreover, the hierarchical architecture improves mechanical strength of the composite, resulting in the formation of flexible binder-free thin film electrode with improved conductivity and enhanced stability upon cycling. All these advantages provide enhanced high rate capability and long-life cycling stability for the composite compared with the pristine one. Combined both good sodium/lithium compatibility and superior electrochemical characteristics, this hierarchical composite can be employed as a high-property cathode material for advanced energy storage devices.

Acknowledgement

This work is supported by the National Natural Science Foundation of China (No. 21001036, 50902041), Fundamental Research Funds for the Central Universities (HEUCF201310011), Program for New Century Excellent Talents in Heilongjiang Provincial University (No. 1253-NCET-012) and Natural Science Foundation of Heilongjiang Province (No. QC2013C008).

Notes and references

^aKey Laboratory of Superlight Material and Surface Technology, Ministry of Education, College of Material Science and Chemical Engineering, Harbin Engineering University, Harbin 150001, Heilongjiang, China; E-Mail: senzhang@hrbeu.edu.cn

^bKey Laboratory for Photonic and Electronic Bandgap Materials, Ministry of Education; College of Chemistry and Chemical Engineering, Harbin Normal University, Harbin, 150025, Heilongjiang, China; E-Mail: chaodenghsd@sina.com

†Electronic Supplementary Information (ESI) available: Description of calculation process for apparent ion diffusion coefficients. The relationship between Z' and ω^{-1/2} of the low-frequency of the Nyquist plots for the Na₇V₄(P₂O₇)₄(PO₄)/C nanorod-graphene composite and the pristine Na₇V₄(P₂O₇)₄(PO₄)/C nanorod. See DOI: 10.1039/b000000x/

- 1 V. Palomares, M. C. Cabanas, E. C. Martinez, M. H. Han, T. Rojo, *Energy Environ. Sci.* **2013**, *6*, 2312.
- 2 D. Wang, D. Choi, J. Li, Z. Yang, Z. Nie, R. Kou, D. Hu, C. Wang, L. Saraf, J. Zhang, I. A. Aksay, J. Liu, *ACS Nano* **2009**, *3*, 907.
- 3 H. Xiong, M. D. Slater, M. Balasubramanian, C. S. Johnson, T. Rajh, *J. Phys. Chem. Lett.* **2011**, *2*, 2560.
- 4 A. K. Padhi, K. S. Nanjundaswamy, J. B. Goodenough, *J. Electrochem. Soc.* **1997**, *144*, 1188.
- 5 A. K. Padhi, K. S. Nanjundaswamy, J. B. Goodenough, *J. Electrochem. Soc.* **1997**, *144*, 1188.
- 6 A. K. Padhi, K. S. Nanjundaswamy, C. Masquelier, S. Okada, J. B. Goodenough, *J. Electrochem. Soc.* **1997**, *144*, 1609.
- 7 M. S. Islam, R. Dominko, C. Masquelier, C. Sirisopanaporn, A. R. Armstrong, P. G. Bruce, *J. Mater. Chem.* **2011**, *21*, 9811.

- 8 C. L. Li, L. Gu, J. W. Tong, J. Maier, *ACS Nano* **2011**, *4*, 2930.
- 9 C. L. Li, C. L. Yin, X. K. Mu, J. Maier, *Chem. Mater.* **2013**, *25*, 962.
- 10 D. J. Kim, Y. H. Jung, K. K. Bharathi, S. H. Je, D. K. Kim, A. Coskun, J. W. Choi, *Adv. Energy Mater.* **2014**, *1400133*.
- 11 X. Y. Wu, Y. L. Cao, X. P. Ai, J. F. Qian, H. X. Yang, *Electrochem. Commun.* **2013**, *31*, 145.
- 12 X. Y. Wu, M. Y. Sun, Y. F. Shen, J. F. Qian, Y. L. Cao, X. P. Ai, H. X. Yan, *ChemSusChem* **2014**, *7*, 407.
- 13 C. Deng, S. Zhang, S. Y. Yang, B. L. Fu, L. Ma, *J. Power Sources* **2011**, *196*, 386.
- 14 L. Tao, G. Rouse, J. N. Chotard, L. Dupont, S. Bruyere, D. Hanzel, G. Mali, R. Dominko, S. Levasseur, C. Masquelier, *J. Mater. Chem. A* **2014**, *2*, 2060.
- 15 P. Barpanda, S. Nishimura, A. Yamada, *Adv. Energy Mater.* **2012**, *2*, 841-859.
- 16 H. Kim, S. Lee, Y. Park, H. Kim, J. Kim, *Chem. Mater.* **2011**, *23*, 3930.
- 17 M. Prabu, M. V. Reddy, S. Selvasekarapandian, G. V. S. Rao, B. V. R. Chowdari, *Electrochim. Acta* **2012**, *85*, 572.
- 18 H. Kim, I. Park, D. H. Seo, S. Lee, S. W. Kim, W. J. Kwon, Y. U. Park, C. S. Kim, S. Jeon, K. Kang, *J. Am. Chem. Soc.* **2012**, *134*, 10369.
- 19 H. Kim, I. Park, S. Lee, H. Kim, K. Y. Park, Y. U. Park, H. Kim, J. Kim, H. D. Lim, W. S. Yoon, K. Kang, *Chem. Mater.* **2013**, *25*, 3614.
- 20 M. Nose, K. Nobuhara, S. Shiotani, H. Nakayama, S. Nakanishi, H. Iba, *RSC Adv.* **2014**, *4*, 9044.
- 21 Q. Kuang, J. T. Xu, Y. M. Zhao, X. L. Chen, L. Q. Chen, *Electrochim. Acta* **2011**, *56*, 2201.
- 22 J. T. Xu, Y. M. Zhao, Q. Kuang, Y. Z. Dong, *Electrochim. Acta* **2011**, *56*, 6562.
- 23 N. Recham, M. C. Cabanas, J. Cabana, C. P. Grey, J. C. Jumas, L. Dupont, M. Armand, J. M. Tarascon, *Chem. Mater.* **2008**, *20*, 6798.
- 24 C. Deng, S. Zhang, Y. H. Sun, Y. Gao, Q. Wu, F. L. Liu, *J. Electrochem. Soc.* **2013**, *160*, A218.
- 25 S. Zhang, C. Deng, H. Gao, F. L. Meng, M. Zhang, *Electrochimica Acta* **2013**, *107*, 406.
- 26 S. Y. Lim, H. Kim, J. Chung, J. H. Lee, B. G. Kim, J. J. Choi, K. Y. Chung, W. Cho, S. J. Kim, W. A. Goddard, Y. S. Jung, J. W. Choi, *PNAS* **2014**, *111*, 599.
- 27 S. Y. Lim, J. W. Choi, *224th ECS Meeting* **2013**, 369
- 28 G. Hautier, A. Jain, H. Chen, C. Moore, S. P. Ong, G. Ceder, *J. Mater. Chem.* **2011**, *21*, 17147
- 29 C. Deng, S. Zhang, Z. Dong, Y. Shang, *Nano Energy* **2014**, *3*, 14.
- 30 J. G. Yu, J. C. Yu, W. K. Ho, L. Wu, X. C. Wang, *J. Am. Chem. Soc.* **2004**, *126*, 3422.
- 31 Q. F. Zhang, E. Uchaker, S. L. Candelaria, G. Z. Cao, *Chem. Soc. Rev.* **2013**, *42*, 3127.
- 32 C. Deng, S. Zhang, *ACS Appl. Mater. Interfaces* **2014**, *6*, 9111.
- 33 Y. Z. Lou, X. Xu, Y. X. Zhang, Y. Q. Pi, Y. L. Zhao, X. C. Tian, Q. Y. An, Q. L. Wei, L. Q. Mai, *Adv. Energy Mater.* DOI: 10.1002/aenm.201400107.
- 34 S. Li, Y. F. Dong, L. Xu, X. Xu, L. He, L. Q. Mai, *Adv. Mater.* **2014**, *26*, 3545-3553.

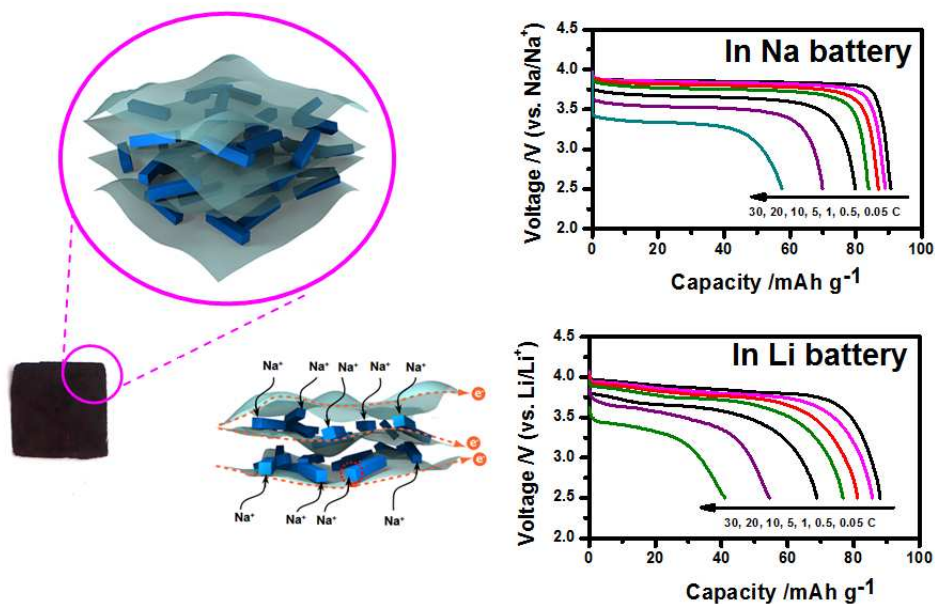
- 35 A. P. Yu, I. Rose, A. Davies, Z. W. Chen, *Appl. Phys. Lett.* **2010**, 96, 253105.
- 36 D. Z. Yang, X. Z. Liao, J. F. Shen, Y. S. He, Z. F. Ma, *J. Mater. Chem. A* **2014**, 2, 6723.
- 5 37 A. P. Yu, H. W. Park, A. Davies, D. C. Higgins, Z. W. Chen, X. C. Xiao, *J. Phys. Chem. Lett.* **2011**, 2, 1855.
- 38 L. Fei, Q. L. Lin, B. Yuan, G. Chen, P. Xie, Y. L. Li, Y. Xu, S. G. Deng, *ACS Appl. Mater. Interfaces* **2013**, 5, 5330.
- 39 S. D. Perera, A. D. Liyanage, N. Nijem, J. P. Ferraris, Y. J. Chabal, 60 46 K. J. B. Jr, *J. Power Sources* **2013**, 230, 130.
- 40 W. X. Song, X. B. Ji, Y. P. Yao, H. J. Zhu, Q. Y. Chen, Q. Q. Sun, C. E. Banks, *Phys. Chem. Chem. Phys.* **2014**, 16, 3055.
- 41 W. X. Song, X. B. Ji, Z. P. Wu, Y. R. Zhu, Y. P. Yao, K. L. Huangfu, Q. Y. Chen, C. E. Banks, *J. Mater. Chem. A* **2014**, 2, 2571.
- 15
- 20
- 25
- 30
- 35
- 40
- 45
- 50
- 55
- 42 W. X. Song, X. B. Ji, C. C. Pan, Y. R. Zhu, Q. Y. Chen, C. E. Banks, *Phys. Chem. Chem. Phys.* **2013**, 15, 14357.
- 43 Barker, J.; Gover, R. K. B.; Burns, P.; Bryan, A. J. *J. Electrochem. Soc.* **2007**, 153, A882-A887.
- 44 B. L. Ellis, W. R. M. Makahnouk, Y. Makimura, K. Toghill, L. F. Nazar, *Nat. Mater.* **2007**, 6, 749
- 45 Q. Cao, H. P. Zhang, G. J. Wang, Q. Xia, Y. P. Wu, H. Q. Wu, *Electrochem. Commun.* **2007**, 9, 1228.
- 46 S. Zhang, C. Deng, B. J. Fu, S. Y. Yang, Li. Ma, *J. Electroanal. Chem.* **2010**, 644, 150.
- 47 A. J. Bard, L. R. Faulkner, *Electrochemical Methods*. Second ed. Wiley. **2001**, 231

Graphic Abstract

Bicontinuous Hierarchical $\text{Na}_7\text{V}_4(\text{P}_2\text{O}_7)_4(\text{PO}_4)/\text{C}$ Nanorod-Graphene Composite with Enhanced Fast Sodium and Lithium Ions Intercalation Chemistry

Sen Zhang^{1,*}, Chao Deng^{2,*}, Yu Meng¹

¹ Key Laboratory of Superlight Material and Surface Technology, Ministry of Education, College of Material Science and Chemical Engineering, Harbin Engineering University, Harbin 150001, Heilongjiang, China; ²Key Laboratory for Photonic and Electronic Bandgap Materials, Ministry of Education, College of Chemistry and Chemical Engineering, Harbin Normal University, Harbin 150025, Heilongjiang, China



Hierarchical $\text{Na}_7\text{V}_4(\text{P}_2\text{O}_7)_4(\text{PO}_4)/\text{C}$ nanorod-graphene composite exhibits enhanced fast sodium/lithium ions transport capability and superb electrochemical property.